

The power-law component of the X-ray emissions from pulsar wind nebulae and their pulsars

Jr-Yue Hsiang,¹ Hsiang-Kuang Chang^{1,2,3} *

¹*Institute of Astronomy, National Tsing Hua University, Hsinchu 30013, Taiwan*

²*Department of Physics, National Tsing Hua University, Hsinchu 30013, Taiwan*

³*Center for Informatics and Computation in Astronomy (CICA), National Tsing Hua University, Hsinchu 30013, Taiwan*

Accepted 2021 January 4. Received 2021 January 4; in original form 2020 September 17

ABSTRACT

To look for possible phenomenological connections between pulsar’s timing properties and emissions from pulsar wind nebulae and their pulsars, we studied the power-law component of the X-ray emissions from 35 pulsar wind nebulae which have a detected pulsar in X-rays. Our major results are in the following: (1) The power-law component of the X-ray luminosities, in the energy range from 0.5 keV to 8 keV, of the nebulae and of the pulsar both show a strong correlation with the pulsar spin-down power (\dot{E}), consistent with earlier studies. However, equally significant correlations with the magnetic field strength at the light cylinder (B_{lc}) are also found. The similar significance level of the correlations with \dot{E} and with B_{lc} suggests that not only \dot{E} but also B_{lc} plays an important role in understanding these power-law emissions. (2) Thermal X-ray emissions are detected in 12 pulsars among the 35 samples. With derived temperature as one additional variable, we found that the photon indices of pulsar’s non-thermal X-ray power-law spectra can be well described by a linear function of $\log P$, $\log \dot{P}$ and temperature logarithm $\log T$. It indicates that the surface temperature of neutron stars plays an important role in determining the energy distribution of the radiating pair plasma in pulsar’s magnetospheres.

Key words: radiation mechanisms: non-thermal – star: neutron – pulsars: general – ISM: supernova remnants – X-ray: ISM – X-ray: stars

1 INTRODUCTION

Pulsar wind nebulae (PWN) are observed across the electromagnetic spectrum from radio bands to very high energy gamma rays. They are extended sources powered by the embedded pulsar through its magnetized winds. These winds are energetic charged particles, most likely electron-positron pairs, flowing out from pulsar’s magnetosphere. When they encounter the relatively slow-moving supernova ejecta, or the interstellar medium if the supernova remnant is no longer around, a pulsar wind nebula shock and a reverse one, called the termination shock, are formed (e.g. Slane (2017)). It is generally believed that the wind is Poynting-dominated when just leaving the magnetosphere, that is, its energy density is dominated by the Poynting flux rather than by particles. The wind, however, becomes particle-dominated when approaching the termination shock (Kennel & Coroniti 1984). It was suggested that, based on a one-zone, shocked wind model, the nebula X-ray luminosity $L_{X,pwn}$ depends on the central pulsar’s spin-down power \dot{E} as $L_{X,pwn} \propto \dot{E}^{\alpha/2}$,

where $-\alpha$ is the power index of the power-law energy distribution of the emitting particles (Chevalier 2000; Cheng, Taam & Wang 2004). We note that, however, mechanisms of accelerating wind particles are a subject of investigation. It was argued that Fermi acceleration at the termination shock is not able to produce particles energetic enough to explain the observed synchrotron radiation in X-ray bands and beyond. Instead, magnetic reconnection way ahead of or around the termination shock was proposed to be the mechanism of converting magnetic energy to particles’ energy (Lyubarsky 2003; Sironi, Spitkovsky & Arons 2013). On the other hand, based on the outer-gap model, non-thermal X-ray luminosity of pulsars, $L_{X,psr}$, was predicted to be proportional to pulsar’s spin-down power roughly as $L_{X,psr} \propto \dot{E}^{1.15}$ with some variations due to different magnetic inclination angles (Cheng, & Zhang 1999; Cheng, Taam & Wang 2004). It is therefore of interest to compare observations of X-ray luminosities from the nebula and from pulsar’s magnetosphere with these model predictions.

Luminosity of X-ray emissions (L_X) from pulsars, sometimes mixed with their PWN, has been indeed found to strongly correlate with pulsar’s spin-down power \dot{E} . In Se-

* E-mail: hkchang@mx.nthu.edu.tw

ward & Wang (1988), with *Einstein* data of nine pulsars, it was found that L_X (0.2 – 4 keV) is proportional to $\dot{E}^{1.39}$, where, the luminosity L_X is contributed from both the pulsar and their nebulae. With *ROSAT* data of 27 pulsars, Becker & Trümper (1997) reported that L_X (0.1 – 2.4 keV) is about $10^{-3}\dot{E}$. This luminosity counts only the emissions from the pulsar. To reduce the contribution from surface thermal emissions, Possenti et al. (2002) considered the energy range of 2 – 10 keV and reported that $L_X \propto \dot{E}^{1.34}$, with a sample of 39 pulsars, whose PWNe, if present, were not separated from their pulsars. Therefore in that study the luminosity includes contribution from PWNe if they exist. Another relation of $L_X \propto \dot{E}^{1.87}$ (2 – 10 keV) was reported in Mattana et al. (2009) for 14 TeV-emitting PWNe, some of which are mixed with pulsar’s luminosity.

In the works mentioned above, there seems to be an indication that the relation between the X-ray luminosity L_X and the spin-down power \dot{E} has a larger power index when emissions from PWNe are included and a smaller one when only the emission from the pulsar is considered. Indeed, in Cheng, Taam & Wang (2004), with a sample of 23 pulsars in the energy range between 2 and 10 keV, the non-pulsed luminosity was found to be $L_X \propto \dot{E}^{1.4}$, while the pulsed one was $L_X \propto \dot{E}^{1.2}$. In Li, Lu & Li (2008), with 24 PWNe and 27 pulsars, it was reported that, in 2 – 10 keV, $L_{X,\text{pwn}} \propto \dot{E}^{1.45}$ and $L_{X,\text{psr}} \propto \dot{E}^{0.92}$, where $L_{X,\text{pwn}}$ is the luminosity from PWNe and $L_{X,\text{psr}}$ is that from pulsars. It is one of the purposes of this paper to examine these relations with a larger sample.

The spectral photon indices Γ_{pwn} and Γ_{psr} in the power-law spectra of the non-thermal X-ray emissions from PWNe and from pulsars are another important property of the emission. With nine bright Crab-like pulsars, relations between Γ_{pwn} and Γ_{psr} , between Γ_{pwn} and \dot{E} , and between Γ_{psr} and \dot{E} were reported (Gotthelf 2003). These relations were, however, not confirmed in Li, Lu & Li (2008) with a larger sample of pulsars and their PWNe. Nonetheless, Cheng, Taam & Wang (2004) reported an indication of a positive correlation between Γ_{pwn} and $L_{X,\text{pwn}}/\dot{E}$, and Li, Lu & Li (2008) found moderately strong positive correlations between Γ_{pwn} and $L_{X,\text{pwn}}$ and between Γ_{pwn} and $L_{X,\text{pwn}}/\dot{E}$. On the other hand, Γ_{psr} was not found to correlate with luminosities or other pulsar timing properties (Cheng, Taam & Wang 2004; Li, Lu & Li 2008).

In this paper, we report correlations among properties of PWN/pulsar power-law component of the X-ray emissions and of pulsars’ rotation, using a sample of 35 PWNe, all with detected pulsars whose X-ray emission can be separated from that of PWNe. To have a more uniform comparison basis, we consider the flux in the energy range from 0.5 keV to 8 keV for all the sources in the sample. This flux is derived from the power-law component of the corresponding best-fit spectral models reported in the literature. It therefore does not include surface thermal emissions (i.e. also excluding the emission ultimately originating from bombardment of electron-positron pairs produced and accelerated in the magnetosphere, see the next section).

Thanks to observations with fine enough spatial resolution and long enough exposure, the X-ray emission from PWNe has been found to become softer with increasing distance from the pulsar, that is, the photon index is larger at a larger distance. Clear examples can be found in Slane

et al. (2012) and Pavan et al. (2016). That certainly represents the cooling of emitting particles in PWNe and deserves detailed study by its own. We therefore decided not to include Γ_{pwn} in our study, and to keep only $L_{X,\text{pwn}}$, $L_{X,\text{psr}}$, and Γ_{psr} as spectral properties of sources in our sample. On the other hand, in studying these possible correlations, we also take the magnetic field strength at the light cylinder and the surface temperature (when available) into account. In particular, the inclusion of the surface temperature leads to a statistically much better description of Γ_{psr} as a linear function of $\log P$, $\log \dot{P}$ and $\log T$.

We describe, in Section 2, how we collect the sample and determine their properties from the literature. In Section 3, results of possible correlations among spectral and timing properties are presented, for the 35 sources in the sample as a whole, and for a subset of 12 samples whose surface temperature estimates are available. Implications of these results are discussed in Section 4.

2 SAMPLE COLLECTION

We collected, from the literature, all the PWNe whose associated pulsars are detected. In this effort, among many different references, we benefited very much from the McGill PWN catalog¹ and Li, Lu & Li (2008). Altogether we found 50, among which 35 have separate X-ray spectral information for PWNe and for their associated pulsars. These 35 are the sources that we study in this work. Their spectral properties are listed in Table 1.

In several earlier studies (Possenti et al. 2002; Cheng, Taam & Wang 2004; Li, Lu & Li 2008) the X-ray luminosity considered was the total luminosity in the energy range of 2 – 10 keV. That luminosity includes contributions of emissions from the nebulae, emissions from pulsars’ magnetosphere, and likely also emissions from the stellar surface due to bombardment of charged particles flowing back from the magnetosphere. The luminosity of the bombardment component presumably may depend on pulsars’ timing properties in a way different from that of the magnetospheric emission. We therefore try to separate them by considering only the flux derived from the best-fit power-law component in corresponding spectral analysis works to represent the component of the magnetospheric emission. In fact, with the caveats above, hereafter we will always identify the power-law component of the X-ray spectra with the non-thermal emission and will use the two terminologies in an interchangeable way. To have a uniform comparison basis, we consider, for all the 35 sources, only the power-law component luminosities in the energy range from 0.5 keV to 8 keV. This energy range is the most common one employed in the spectral analysis we found in the literature, in particular for those based on Chandra data. When fluxes and uncertainties in the literature were reported in a different energy range, we compute the corresponding flux in 0.5 – 8 keV and estimate the uncertainty with the published value scaled by the flux ratio of the two energy ranges. To covert

¹ Roberts, M.S.E., 2004, ‘The Pulsar Wind Nebula Catalog (March 2005 version)’, McGill University, Montreal, Quebec, Canada (available on the World-Wide-Web at ‘http://www.physics.mcgill.ca/~pulsar/pwncat.html’).

Table 1. X-ray spectral properties of 35 PWNe with detected pulsars. References: (1) Slane et al. (2004); (2) Li, Lu & Li (2008); (3) Klingler et al. (2016b); (4) Ge et al. (2019); (5) De Luca et al. (2005); (6) Posselt et al. (2017); (7) Birzan, Pavlov & Kargaltsev (2016); (8) Pavlov et al. (2001); (9) Kargaltsev, Pavlov & Garmire (2007); (10) Pavan et al. (2016); (11) Chang et al. (2012); (12) Ng, Roberts & Romani (2005); (13) Kishishita et al. (2012); (14) Klingler et al. (2016a); (15) DeLaney et al. (2006); (16) Kargaltsev, Pavlov & Wang (2009); (17) Romani et al. (2005); (18) Hinton et al. (2007); (19) Klingler et al. (2018); (20) Roberts et al. (2003); (21) Helfand et al. (2007); (22) Duvidovich et al. (2019); (23) Matheson & Safi-Harb (2010); (24) Gotthelf & Halpern (2008); (25) Petre, Kuntz & Shelton (2002); (26) Temim et al. (2010); (27) Becker et al. (2006); (28) Li, Lu & Li (2005); (29) Van Etten, Romani & Ng (2008); (30) Romani, Slane & Green (2017); (31) Johnson & Wang (2010). [†]PSR J2124-3358 is a millisecond pulsar, which is not included in the selected sample of 35 objects to which the correlation analysis was applied, but is listed here for reference.

Pulsar name	PWN name	$L_{X,\text{pwn}}$ (erg/s)	$L_{X,\text{psr}}$ (erg/s)	Γ_{psr}	kT_{∞} (eV)	References
J0205+6449	G130.7+3.1	$2.26^{+2.22}_{-1.46} \times 10^{34}$	$1.25^{+1.33}_{-0.83} \times 10^{34}$	$2.07^{+0.02}_{-0.02}$	$112.0^{+8.6}_{-8.6}$	1, 2
J0358+5413		$5.89^{+6.00}_{-3.83} \times 10^{31}$	$7.38^{+8.05}_{-4.90} \times 10^{30}$	$1.45^{+0.21}_{-0.24}$	$160.0^{+12.0}_{-12.0}$	3
J0534+2200	G184.6-5.8	$1.89^{+1.99}_{-1.24} \times 10^{37}$	$1.32^{+1.89}_{-0.97} \times 10^{36}$	$1.63^{+0.09}_{-0.09}$	–	2
J0537-6910	G279.6-31.7	$2.09^{+2.60}_{-1.45} \times 10^{36}$	$7.43^{+14.00}_{-5.54} \times 10^{35}$	$1.80^{+0.20}_{-0.20}$	–	2
J0540-6919	G279.7-31.5	$1.43^{+1.38}_{-0.92} \times 10^{37}$	$3.02^{+3.36}_{-2.01} \times 10^{36}$	$0.78^{+0.09}_{-0.09}$	–	4
J0633+1746	G195.1+4.3	$3.37^{+3.49}_{-2.21} \times 10^{29}$	$1.48^{+1.46}_{-1.02} \times 10^{30}$	$1.47^{+0.06}_{-0.07}$	$83.4^{+4.2}_{-4.2}$	5, 6
J0659+1414		$8.35^{+19.30}_{-6.94} \times 10^{28}$	$1.51^{+2.83}_{-1.07} \times 10^{30}$	$2.30^{+0.68}_{-0.57}$	$93.1^{+4.6}_{-7.3}$	7
J0835-4510	G263.9-3.3	$7.14^{+7.76}_{-4.74} \times 10^{32}$	$2.20^{+2.70}_{-1.52} \times 10^{32}$	$2.20^{+0.40}_{-0.40}$	$130.1^{+2.6}_{-2.6}$	2, 8
J1016-5857	G284.3-1.8	$2.00^{+2.89}_{-1.46} \times 10^{32}$	$5.00^{+2.00}_{-2.00} \times 10^{31}$	$1.50^{+0.40}_{-0.40}$	–	9
J1048-5832	G287.4+0.58	$6.60^{+7.52}_{-4.44} \times 10^{31}$	$2.60^{+0.40}_{-0.40} \times 10^{31}$	$1.50^{+0.30}_{-0.30}$	–	9
J1101-6101	IGRJ11014-6103	$7.43^{+7.37}_{-4.80} \times 10^{33}$	$3.53^{+3.56}_{-2.29} \times 10^{33}$	$1.08^{+0.08}_{-0.08}$	–	10
J1124-5916	G292.0+1.8	$3.14^{+5.01}_{-2.29} \times 10^{34}$	$2.66^{+4.09}_{-1.91} \times 10^{33}$	$1.62^{+0.10}_{-0.10}$	–	2
J1357-6429		$2.24^{+3.10}_{-1.60} \times 10^{32}$	$7.27^{+14.90}_{-5.41} \times 10^{31}$	$1.72^{+0.55}_{-0.63}$	$140.0^{+60.0}_{-40.0}$	11
J1420-6048	G313.6+0.3	$3.39^{+3.41}_{-2.20} \times 10^{34}$	$4.63^{+8.62}_{-3.73} \times 10^{32}$	$1.00^{+4.20}_{-4.80}$	–	12, 13
J1509-5850		$1.22^{+1.23}_{-0.79} \times 10^{33}$	$7.14^{+5.51}_{-4.72} \times 10^{31}$	$1.90^{+0.12}_{-0.12}$	–	14
J1513-5908	G320.4-1.2	$1.35^{+1.64}_{-0.93} \times 10^{35}$	$9.86^{+16.20}_{-7.54} \times 10^{34}$	$1.19^{+0.04}_{-0.04}$	–	15
J1617-5055		$1.84^{+2.14}_{-1.25} \times 10^{33}$	$9.52^{+9.21}_{-6.10} \times 10^{33}$	$1.14^{+0.06}_{-0.06}$	–	16
J1709-4429	G343.1-2.3	$1.21^{+1.21}_{-0.78} \times 10^{33}$	$1.82^{+1.92}_{-1.19} \times 10^{32}$	$1.62^{+0.20}_{-0.20}$	$172.3^{+14.6}_{-13.8}$	17
J1718-3825		$2.93^{+5.68}_{-2.40} \times 10^{32}$	$2.43^{+4.72}_{-1.99} \times 10^{32}$	$1.47^{+0.21}_{-0.21}$	–	18
J1747-2958	G359.23-0.82	$5.15^{+5.05}_{-3.32} \times 10^{33}$	$1.48^{+1.77}_{-1.01} \times 10^{33}$	$1.55^{+0.04}_{-0.04}$	–	19
J1801-2451	G5.27-0.9	$2.12^{+3.28}_{-1.58} \times 10^{32}$	$1.54^{+1.70}_{-1.03} \times 10^{33}$	$1.60^{+0.60}_{-0.50}$	–	9
J1803-2137		$2.00^{+2.30}_{-1.35} \times 10^{32}$	$6.76^{+8.38}_{-4.67} \times 10^{31}$	$1.40^{+0.60}_{-0.60}$	$200.0^{+100.0}_{-100.0}$	9
J1809-1917		$8.60^{+10.20}_{-5.86} \times 10^{32}$	$3.23^{+5.15}_{-2.38} \times 10^{31}$	$1.23^{+0.62}_{-0.62}$	$170.0^{+30.0}_{-30.0}$	19
J1811-1925	G11.2-0.3	$1.70^{+1.71}_{-1.10} \times 10^{34}$	$6.97^{+7.27}_{-4.57} \times 10^{33}$	$0.97^{+0.32}_{-0.39}$	–	20
J1813-1749	G12.82-0.02	$2.55^{+4.95}_{-2.09} \times 10^{34}$	$5.92^{+11.49}_{-4.85} \times 10^{33}$	$1.3^{+0.30}_{-0.30}$	–	21
J1826-1334	G18.0-0.7	$2.09^{+2.13}_{-1.36} \times 10^{33}$	$1.78^{+1.89}_{-1.17} \times 10^{32}$	$1.26^{+0.25}_{-0.25}$	–	22
J1833-1034	G21.5-0.9	$2.35^{+2.78}_{-1.60} \times 10^{34}$	$9.05^{+12.20}_{-6.44} \times 10^{33}$	$1.14^{+0.05}_{-0.07}$	$520.0^{+30.0}_{-40.0}$	23
J1838-0655		$6.73^{+11.57}_{-5.25} \times 10^{32}$	$3.55^{+3.92}_{-2.36} \times 10^{34}$	$0.50^{+0.20}_{-0.20}$	–	24
J1856+0113	G34.7-0.4	$6.80^{+8.11}_{-4.63} \times 10^{32}$	$1.08^{+1.59}_{-0.78} \times 10^{32}$	$1.28^{+0.48}_{-0.48}$	–	25
J1930+1852	G54.1+0.3	$5.31^{+10.30}_{-4.36} \times 10^{34}$	$1.55^{+3.00}_{-1.27} \times 10^{34}$	$1.20^{+0.20}_{-0.20}$	–	26
J1932+1059	G47.4-3.9	$6.13^{+18.60}_{-4.84} \times 10^{29}$	$2.97^{+3.11}_{-1.96} \times 10^{30}$	$2.72^{+0.12}_{-0.09}$	–	27
J1952+3252	G69.0+2.7	$7.86^{+8.35}_{-5.18} \times 10^{33}$	$2.91^{+3.28}_{-1.95} \times 10^{33}$	$1.63^{+0.03}_{-0.05}$	$130.0^{+2.0}_{-2.0}$	28
J2021+3651	G75.2+0.1	$6.82^{+7.11}_{-4.47} \times 10^{33}$	$6.34^{+7.33}_{-4.29} \times 10^{32}$	$1.73^{+1.15}_{-1.02}$	$159.4^{+17.2}_{-20.6}$	29
J2124-3358 [†]		$3.34^{+3.35}_{-2.16} \times 10^{29}$	$2.80^{+2.84}_{-1.82} \times 10^{29}$	$2.50^{+0.20}_{-0.10}$	$250.0^{+10.0}_{-10.0}$	30
J2225+6535	G108.6+6.8	$4.53^{+5.57}_{-3.25} \times 10^{30}$	$1.45^{+1.73}_{-1.03} \times 10^{30}$	$1.70^{+0.46}_{-0.23}$	–	31
J2229+6114	G106.6+3.1	$4.04^{+7.83}_{-3.06} \times 10^{32}$	$3.82^{+6.30}_{-2.70} \times 10^{32}$	$1.05^{+0.10}_{-0.10}$	–	2

fluxes into luminosities, distances to the sources are needed. We adopt the best-estimate distances provided in the ATNF pulsar catalog² for the conversion. Following Possenti et al. (2002) and Li, Lu & Li (2008), we also adopt an uncertainty of $\pm 40\%$ in distances. For most of the cases, this is in fact the dominating uncertainty in determining luminosities. These distances and other pulsar timing properties are listed in Table 2.

Among these 35 pulsars, thermal emissions are detected in 12 of them, in addition to the non-thermal power-law component. These are thermal emissions from neutron stars' surface, which reveal information about the surface temperatures. Because of the presence of strong magnetic fields and the anisotropy of thermal conductivity, the surface temperature is higher near magnetic poles. Furthermore, possible charged-particle bombardment on the polar cap region heats the magnetic polar region further. Thermal emissions from the non-uniform surface temperature distribution is very often dominated by the hot polar region. In spectral analysis, besides the power-law component, one usually employs a black-body component to describe the thermal emissions if that improves the spectral fitting statistically. Sometimes two black-body components, representing a hot spot at the magnetic pole and a cooler stellar surface outside the hot spot, are used when further improvement can be obtained. Some authors also use neutron-star atmospheric emission models to fit the thermal emissions. Surface thermal emissions may affect the production of electron-positron pairs and their energy distribution, either in the outer gap (e.g. Cheng, Ho & Ruderman (1986); Takata & Chang (2009)) or above the polar cap (e.g. Chang (1995); Sturmer (1995); Harding & Muslimov (1998); Timokhin & Harding (2019)). That in turn will affect spectral properties of non-thermal emissions from pulsars' magnetosphere. Since the black-body model has been applied in all the 12 sources in the literature, we use the surface temperatures inferred from the best-fit black-body component for our correlation analysis. For the cases of best fit with two black-body components (PSR J0633+1746 and PSR J0659+1414), a flux-weighted average temperature is employed. These temperatures are listed in Table 1 (in the ' kT_∞ ' column, where T_∞ is the temperature inferred from the measured spectrum and k is the Boltzmann constant).

For the convenience of future investigation, pulsars with detected PWNe but not included in this study for various reasons are listed in the following: (1) PWNe or pulsars too dim in X-rays to separate their X-ray emission – PSR J0437-4715 (Bogdanov 2013; Guillot et al. 2016; Bogdanov et al. 2019), PSR J0538+2817 (Romani & Ng 2003; McGowan et al. 2003; Ng et al. 2007), PSR J1028-5819 (Mignani et al. 2012), PSR J1057-5226 (Posselt, Spence & Pavlov 2015), PSR J1301-6305 (Abramowski et al. 2012), PSR J1648-4611 (Sakai et al. 2013), PSR J1702-4128 (Chang, Konopelko & Cui 2008), PSR J1831-0952 (Abichandani et al. 2019); (2) Pulsars with magnetar-like bursts – PSR J1119-6127 (Blumer, Safi-Harb & McLaughlin 2017; Lin et al. 2018; Dai et al. 2018; Archibald et al. 2018), PSR J1846-0258 (Kuiper, Hermsen & Dekker 2018; Reynolds, Borkowski & Gwynne 2018; Temim et al. 2019); (3) A black-widow pul-

sar, whose X-ray emission is from an intrabinary shock – PSR J1959+2048 (Huang et al. 2012; Kandel, Romani & An 2019); (4) An old millisecond pulsar appearing as an outlier in P and \dot{P} distributions – PSR J2124-3358 (Romani, Slane & Green 2017); (5) No reported X-ray emissions – PSR J0908-4913 (Gaensler et al. 1998; Stappers, Gaensler & Johnston 1999), PSR J1341-6220 (Wilson 1986; Caswell et al. 1992; Kaspi et al. 1992), PSR J1646-4346 (Giacani et al. 2001). More PWNe whose pulsars have not yet been detected can be found in the McGill PWN Catalog. We note that, for the two pulsars with magnetar-like bursts, the X-ray luminosities, both of the nebulae and of the pulsars, were observed to vary (Blumer, Safi-Harb & McLaughlin 2017; Reynolds, Borkowski & Gwynne 2018). Those emissions may come from a mixture of mechanisms powered by pulsar's rotation and strong magnetic fields. PSR J2124-3358 is a millisecond pulsar. Its non-thermal X-ray luminosity may depend on the timing properties in a way different from normal pulsars, because of its weak magnetic field (e.g. Zhang & Cheng (2003)). This pulsar is still included in all the figures for reference.

3 CORRELATIONS BETWEEN SPECTRAL AND TIMING PROPERTIES

We first examine possible correlations between non-thermal X-ray luminosities ($L_{X,\text{pwn}}, L_{X,\text{psr}}$) and pulsar timing properties. The latter include period P , period time-derivative \dot{P} , spin-down power \dot{E} , characteristic age τ , the dipole magnetic field strength at the stellar surface B_s and at the light cylinder B_{lc} . We adopt conventional values of the moment of inertia $I = 10^{45}$ g cm² and radius $R = 10$ km for the pulsar, and have (all in gaussian units) $\dot{E} = I\Omega\dot{\Omega} = 3.9 \times 10^{46} P^{-3} \dot{P}$, $\tau = 0.5 P \dot{P}^{-1}$, $B_s = 3.2 \times 10^{19} (P \dot{P})^{0.5}$, and $B_{\text{lc}} = B_s (R/R_{\text{lc}})^3 = 2.9 \times 10^8 P^{-2.5} \dot{P}^{0.5}$, where $\Omega = 2\pi/P$ and the light cylinder radius $R_{\text{lc}} = c/\Omega$. They are plotted in Fig.1, 2 and 3. We use the Spearman rank-order correlation coefficient r_s to indicate the significance of possible correlations. Each r_s and its associated random probability p are noted in the figures.

As found in earlier literature, these luminosities are strongly correlated with \dot{E} (Fig. 2). We found, however, their correlations with B_{lc} are also equally strong (Fig. 3). The best fits to these correlations, using the least-square method to fit a linear function of the logarithms of these variables, are

$$L_{X,\text{pwn}} \propto \dot{E}^{1.32 \pm 0.13} \quad (\chi_\nu^2 = 4.38) , \quad (1)$$

$$L_{X,\text{pwn}} \propto B_{\text{lc}}^{1.83 \pm 0.19} \quad (\chi_\nu^2 = 4.59) , \quad (2)$$

$$L_{X,\text{psr}} \propto \dot{E}^{1.15 \pm 0.11} \quad (\chi_\nu^2 = 3.43) , \quad (3)$$

and

$$L_{X,\text{psr}} \propto B_{\text{lc}}^{1.59 \pm 0.17} \quad (\chi_\nu^2 = 3.81) . \quad (4)$$

The fitting uncertainties reported here and hereafter are all at a confidence level of 68%. The reduced chi-squares of these best fits are large and statistically not acceptable. It reflects the fact that there is a huge scatter among data points in those corresponding figures, although correlations seem strong. We note that, in this work, best fits and chi-squares are only suggestive, because the quoted uncertain-

² <https://www.atnf.csiro.au/research/pulsar/psrcat/>

Table 2. Properties of the 35 pulsars employed in our analysis. Surface temperature information is available for 12 of them. †PSR J2124-3358 is a millisecond pulsar, which is not included in the selected sample of 35 objects to which the correlation analysis was applied, but is listed here for reference.

Source name	Distance (kpc)	P (s)	\dot{P} (s/s)	\dot{E} (erg/s)	τ (yr)	B_s (G)	B_{1c} (G)
J0205+6449	3.20	0.0657	1.94×10^{-13}	2.7×10^{37}	5.37×10^3	3.61×10^{12}	1.19×10^5
J0358+5413	1.00	0.1564	4.40×10^{-15}	4.5×10^{34}	5.64×10^5	8.39×10^{11}	2.06×10^3
J0534+2200	2.00	0.0330	4.21×10^{-13}	4.5×10^{38}	1.26×10^3	3.79×10^{12}	9.55×10^5
J0537-6910	49.70	0.0161	5.18×10^{-14}	4.9×10^{38}	4.93×10^3	9.25×10^{11}	2.07×10^6
J0540-6919	49.70	0.0505	4.79×10^{-13}	1.5×10^{38}	1.67×10^3	4.98×10^{12}	3.61×10^5
J0633+1746	0.19	0.2371	1.10×10^{-14}	3.2×10^{34}	3.42×10^5	1.63×10^{12}	1.15×10^3
J0659+1414	0.29	0.3849	5.49×10^{-14}	3.8×10^{34}	1.11×10^5	4.65×10^{12}	7.65×10^2
J0835-4510	0.28	0.0893	1.25×10^{-13}	6.9×10^{36}	1.13×10^4	3.38×10^{12}	4.45×10^4
J1016-5857	3.16	0.1074	8.08×10^{-14}	2.6×10^{36}	2.10×10^4	2.98×10^{12}	2.26×10^4
J1048-5832	2.90	0.1237	9.61×10^{-14}	2.0×10^{36}	2.04×10^4	3.49×10^{12}	1.73×10^4
J1101-6101	7.00	0.0630	8.60×10^{-15}	1.4×10^{36}	1.16×10^5	7.42×10^{11}	2.81×10^4
J1124-5916	5.00	0.1350	7.53×10^{-13}	1.2×10^{37}	2.85×10^3	1.02×10^{13}	3.85×10^4
J1357-6429	3.10	0.1661	3.60×10^{-13}	3.1×10^{36}	7.31×10^3	7.83×10^{12}	1.60×10^4
J1420-6048	5.63	0.0682	8.32×10^{-14}	1.0×10^{37}	1.30×10^4	2.41×10^{12}	7.13×10^4
J1509-5850	3.37	0.0889	9.17×10^{-15}	5.1×10^{35}	1.54×10^5	9.14×10^{11}	1.22×10^4
J1513-5908	4.40	0.1513	1.53×10^{-12}	1.7×10^{37}	1.57×10^3	1.54×10^{13}	4.15×10^4
J1617-5055	4.74	0.0694	1.35×10^{-13}	1.6×10^{37}	8.13×10^3	3.10×10^{12}	8.70×10^4
J1709-4429	2.60	0.1020	9.30×10^{-14}	3.4×10^{36}	1.75×10^4	3.12×10^{12}	2.72×10^4
J1718-3825	3.49	0.0747	1.32×10^{-14}	1.3×10^{36}	8.95×10^4	1.01×10^{12}	2.26×10^4
J1747-2958	2.52	0.0988	6.13×10^{-14}	2.5×10^{36}	2.55×10^4	2.49×10^{12}	2.42×10^4
J1801-2451	3.80	0.1249	1.28×10^{-13}	2.6×10^{36}	1.55×10^4	4.04×10^{12}	1.95×10^4
J1803-2137	4.40	0.1337	1.34×10^{-13}	2.2×10^{36}	1.58×10^4	4.29×10^{12}	1.68×10^4
J1809-1917	3.27	0.0827	2.55×10^{-14}	1.8×10^{36}	5.14×10^4	1.47×10^{12}	2.43×10^4
J1811-1925	5.00	0.0646	4.40×10^{-14}	6.4×10^{36}	2.33×10^4	1.71×10^{12}	5.92×10^4
J1813-1749	4.70	0.0447	1.27×10^{-13}	5.6×10^{37}	5.60×10^3	2.41×10^{12}	2.53×10^5
J1826-1334	3.61	0.1010	7.53×10^{-14}	2.8×10^{36}	2.14×10^4	2.80×10^{12}	2.51×10^4
J1833-1034	4.10	0.0619	2.02×10^{-13}	3.4×10^{37}	4.85×10^3	3.58×10^{12}	1.42×10^5
J1838-0655	6.60	0.0705	4.93×10^{-14}	5.5×10^{36}	2.27×10^4	1.89×10^{12}	5.05×10^4
J1856+0113	3.30	0.2674	2.08×10^{-13}	4.3×10^{35}	2.03×10^4	7.55×10^{12}	3.70×10^3
J1930+1852	7.00	0.1369	7.51×10^{-13}	1.2×10^{37}	2.89×10^3	1.03×10^{13}	3.75×10^4
J1932+1059	0.31	0.2265	1.16×10^{-15}	3.9×10^{33}	3.10×10^6	5.18×10^{11}	4.18×10^2
J1952+3252	3.00	0.0395	5.84×10^{-15}	3.7×10^{36}	1.07×10^5	4.86×10^{11}	7.38×10^4
J2021+3651	10.51	0.1037	9.57×10^{-14}	3.4×10^{36}	1.72×10^4	3.19×10^{12}	2.68×10^4
J2124-3358†	0.41	0.0049	7.27×10^{-21}	2.36×10^{33}	1.07×10^{10}	1.92×10^8	1.50×10^4
J2225+6535	0.83	0.6825	9.66×10^{-15}	1.2×10^{33}	1.12×10^6	2.60×10^{12}	7.66×10^1
J2229+6114	3.00	0.0516	7.83×10^{-14}	2.2×10^{37}	1.05×10^4	2.03×10^{12}	1.39×10^5

ties are dominated by distance uncertainties and are not derived rigorously with proper statistics. These unacceptable best fits are similar to what were found in earlier literature (e.g. Possenti et al. (2002); Li, Lu & Li (2008)). The correlations of these luminosities with P and with τ are weaker,

and much weaker with \dot{P} . They are uncorrelated with B_s , as indicated by the Spearman's coefficient shown in Fig. 3.

Although the magnitude of the fitting uncertainties to the best-fit power indices in Eq.(1) and Eq.(3) make the two power indices indistinguishable, the trend that $L_{X,pwn}$ depends on \dot{E} with a larger power index than $L_{X,psr}$ does, as

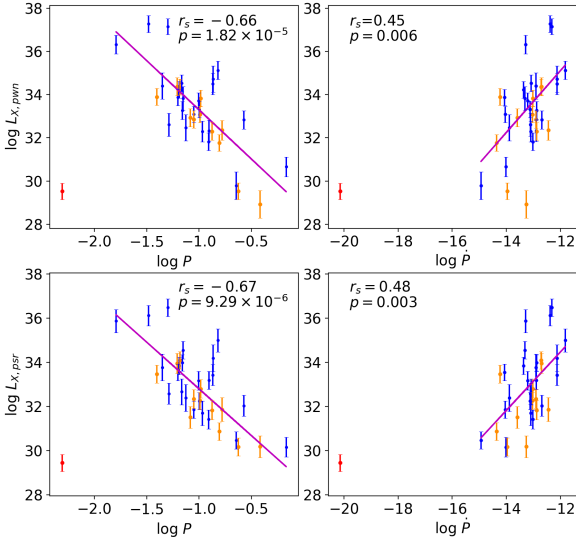


Figure 1. Luminosity of PWNe ($L_{X,\text{pwn}}$, upper panels) and of pulsars ($L_{X,\text{psr}}$, lower panels) versus pulsar period (P , left panels) and period time derivative (\dot{P} , right panels). In the legend, r_s is the Spearman rank-order correlation coefficient and p is the corresponding random probability. The 12 data points in orange are those with detected surface thermal emissions. The purple lines are the best-fit linear function for the 23 data points in blue and 12 in orange. The red data point is PSR J2124-3358, which is a millisecond pulsar and is not included in determining r_s and the linear fitting. All the quantities are in gaussian units.

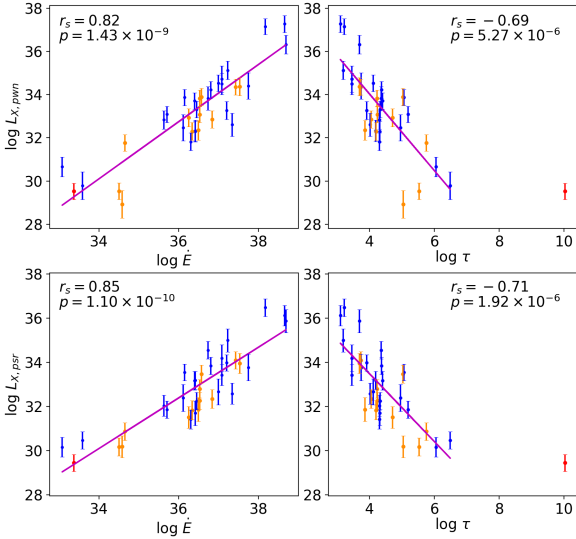


Figure 2. The same as Fig. 1 but for $L_{X,\text{pwn}}$ and $L_{X,\text{psr}}$ versus pulsar's spin-down power (\dot{E} , left panels) and characteristic age (τ , right panels).

mentioned in Section 1, is still present. On the other hand, \dot{E} and B_{lc} seem to play equally important roles in these correlations, when treated separately. It is tempting that both factors should be taken into account together. We therefore checked whether a two-variable fitting gives a better description. The best fits of $\log L_{X,\text{pwn}}$ and $\log L_{X,\text{psr}}$ as a linear function of $\log \dot{E}$ and $\log B_{\text{lc}}$ are

$$L_{X,\text{pwn}} \propto \dot{E}^{0.83 \pm 0.52} B_{\text{lc}}^{0.71 \pm 0.73} \quad (\chi^2_\nu = 4.38) \quad (5)$$

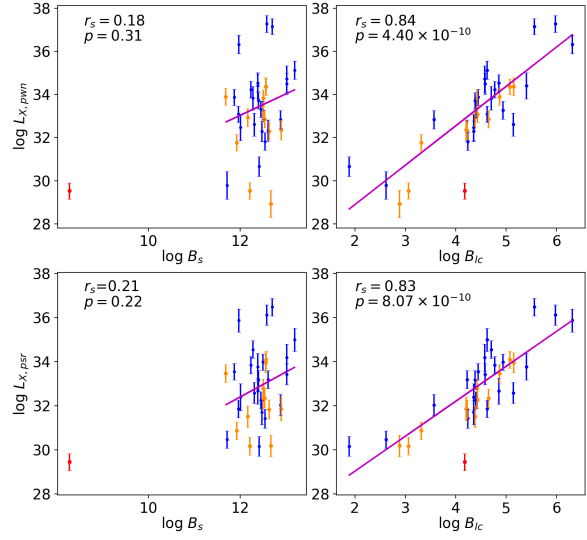


Figure 3. The same as Fig. 1 but for $L_{X,\text{pwn}}$ and $L_{X,\text{psr}}$ versus pulsar's dipole magnetic field strength at the surface (B_s , left panels) and at the light cylinder (B_{lc} , right panels).

and

$$L_{X,\text{psr}} \propto \dot{E}^{0.93 \pm 0.48} B_{\text{lc}}^{0.32 \pm 0.68} \quad (\chi^2_\nu = 3.51) \quad (6)$$

Based on the reported χ^2_ν in these best fits and those in Eq.(1) – Eq.(4), it is clear that the fitting is not improved by invoking two variables. Furthermore, the fitting uncertainties become too large to distinguish the dependence of $L_{X,\text{pwn}}$ and $L_{X,\text{psr}}$ on \dot{E} and B_{lc} .

Since \dot{E} and B_{lc} are simply functions of P and \dot{P} , we also fit luminosity logarithms as a linear function of $\log P$ and $\log \dot{P}$ directly. The best fits are

$$L_{X,\text{pwn}} \propto P^{-4.21 \pm 0.54} \dot{P}^{1.10 \pm 0.24} \quad (\chi^2_\nu = 4.46) \quad (7)$$

and

$$L_{X,\text{psr}} \propto P^{-3.74 \pm 0.49} \dot{P}^{1.00 \pm 0.21} \quad (\chi^2_\nu = 3.47) \quad (8)$$

With $\dot{E} \propto P^{-3} \dot{P}$ and $B_{\text{lc}} \propto P^{-2.5} \dot{P}^{0.5}$, the above equations can be expressed in terms of \dot{E} and B_{lc} as the following:

$$L_{X,\text{pwn}} \propto \dot{E}^{0.65 \pm 0.66} B_{\text{lc}}^{0.91 \pm 0.90} \quad (9)$$

and

$$L_{X,\text{psr}} \propto \dot{E}^{0.63 \pm 0.58} B_{\text{lc}}^{0.74 \pm 0.80} \quad (10)$$

In view of the large fitting uncertainties, the above two equations are not inconsistent with Eq.(5) and Eq.(6).

The non-thermal luminosity of PWNe and of pulsars depends in a similar way on timing properties. Among the 35 neutron stars studied in this paper, 29 $L_{X,\text{pwn}}$ are larger than the corresponding $L_{X,\text{psr}}$. The ratio $L_{X,\text{pwn}}/L_{X,\text{psr}}$, that is, the flux ratio $F_{X,\text{pwn}}/F_{X,\text{psr}}$, ranges from 0.06 to 73. This ratio, however, is not found to correlate with any timing properties. One example, the relation between this ratio and \dot{E} , is shown in Figure 4, in which one can see that their correlation is very weak. This ratio is not consistent with a constant either. The linear best fit shown in Figure 4, with a slope of -0.02 ± 0.10 and a reduced chi-square equal to 120, is statistically unacceptable.

The photon index of the non-thermal X-ray power-law

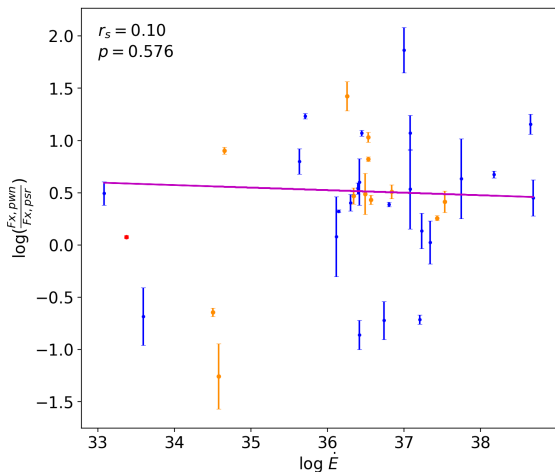


Figure 4. X-ray flux ratio of nebulae to pulsars versus \dot{E} . The purple line is the linear best fit, which has a slope of -0.02 ± 0.10 but is unacceptable ($\chi^2_\nu = 120$).

spectrum of the 35 pulsars we studied is not correlated with any timing properties. The most significant Spearman’s correlation coefficient is 0.29 (random probability 0.09) for Γ_{psr} versus $\log P$ and -0.30 versus $\log B_{\text{lc}}$. The best fits to Γ_{psr} as a linear function of logarithm of a single timing variable all yield a reduced chi-square of about 29, which is large, as expected from the very weak correlations. So is the fit to Γ_{psr} as a linear function of two variables, $\log P$ and $\log \dot{P}$, together. However, with the subset of 12 samples whose surface temperature estimate is observationally available (Table 1), we found that the correlation between Γ_{psr} and the surface temperature logarithm $\log T$ is modestly strong, at a Spearman’s correlation coefficient of -0.69 (random probability 0.01, Fig. 5). Its best-fit function is

$$\Gamma_{\text{psr}} = 4.32^{+0.66}_{-0.66} - 1.23^{+0.31}_{-0.31} \log T \quad (\chi^2_\nu = 9.55) \quad , \quad (11)$$

where, and hereafter, T is in units of eV/k. The reduced chi-square χ^2_ν is still statistically unacceptable.

The photon index of this 12-sample subset is not too different from the whole 35-sample set. Its correlations with timing variables and best-fit reduced chi-squares are all similar to that of the whole sample, as described in the last paragraph. As revealed in Fig. 1 – Fig. 3, these 12 pulsars do not form a separate population. When the surface temperature T is taken into account, nonetheless, the fitting is significantly improved, with reduced chi-squares χ^2_ν decreasing from between 22 and 32 when fitting without T to between 0.65 and 8.43 when T is included. The most significant one is

$$\begin{aligned} \Gamma_{\text{psr}} = & 8.21^{+0.56}_{-0.56} - 1.40^{+0.11}_{-0.11} \log T \\ & - 0.61^{+0.09}_{-0.09} \log P + 0.31^{+0.03}_{-0.03} \log \dot{P} \\ & (\chi^2_\nu = 0.65) \quad . \end{aligned} \quad (12)$$

Without T , the best fit of Γ_{psr} as a linear function of $\log P$ and $\log \dot{P}$ is $\Gamma_{\text{psr}} = 5.07^{+1.89}_{-1.89} - 0.24^{+0.51}_{-0.51} \log P + 0.27^{+0.14}_{-0.14} \log \dot{P}$, with a reduced chi-square $\chi^2_\nu = 25.12$ for 9 degrees of freedom. The F statistic for adding one more vari-

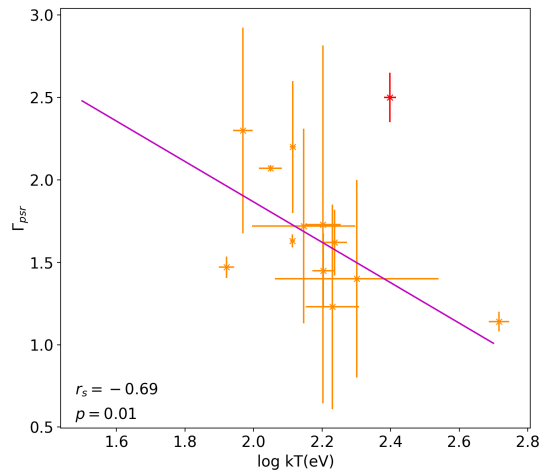


Figure 5. The same as Fig. 1 but with pulsar’s photon indices (Γ_{psr}) versus surface temperatures (T). The orthogonal distance regression method is employed for the fitting.

able, i.e. $\log T$, is $F = \Delta\chi^2/\chi^2_\nu = (25.12 \times 9 - 0.65 \times 8)/0.65 \approx 340$, corresponding to a p value way below 10^{-5} , indicating a very significant improvement of the fitting. This equation suggests a possible dependence of Γ_{psr} on T , P and \dot{P} as the following:

$$\begin{aligned} \Gamma_{\text{psr}} &= 8.21 + \log(T^{-1.40} P^{-0.61} \dot{P}^{0.31}) \\ &\approx 8.21 + \log(T^{-\frac{3}{2}} P^{-\frac{2}{3}} \dot{P}^{\frac{1}{3}}) \quad . \end{aligned} \quad (13)$$

The combination of P and \dot{P} to certain powers can always be turned into a combination of any two timing variables. Unlike the case of $L_{X,\text{pwn}}$ and $L_{X,\text{psr}}$, we do not see Γ_{psr} correlate more with any particular timing variable. We therefore keep the factor $P^{-\frac{2}{3}} \dot{P}^{\frac{1}{3}}$ here, awaiting more physical interpretations.

4 DISCUSSION

The scatter of data point distribution in Fig. 1–5 is quite large, even for the cases with stronger correlations, such as $L_{X,\text{pwn}}$ versus \dot{E} and B_{lc} , and $L_{X,\text{psr}}$ versus \dot{E} and B_{lc} . This may indicate there are other dependences missing in these figures and may also be due to huge uncertainties in the spectral properties of the samples that we collect. These uncertainties include that from the original observations, from our choice of the nebula regions for PWNe with complex morphology, and, most importantly, from the distance estimate. In addition, emissions from pulsars are probably viewing-geometry dependent. The luminosity $L_{X,\text{psr}}$ derived from the observed flux does not necessarily represent the true luminosity of the pulsar in question. Emissions from PWNe are even more complicated. They depend not only on properties of pulsar winds, but also on properties of the environments (e.g. Kolb et al. (2017)). Nonetheless, some intriguing correlations between these luminosities and pulsars’ timing variables do exist.

The correlation between X-ray luminosities and the

spin-down power \dot{E} has been extensively studied in the literature, as briefly reviewed in Section 1. With a larger sample than before, we obtain similar results. Possible dependence on the magnetic field strength at the light cylinder, however, was somehow overlooked in earlier studies. If pulsars' non-thermal X-ray emission comes from a region close to the light cylinder, the magnetic field strength there will very likely affect the X-ray luminosity. The nebula emission, presumably synchrotron radiation in nature, depends on energetics of charged particles in the pulsar winds and on the magnetic field strength around the termination shock. If these charged particles are accelerated by magnetic reconnection, no matter along the way from the light cylinder to the termination shock or close to the termination shock, the field strength at the light cylinder may matter in some way. It is therefore not surprising to see $L_{X,\text{pwn}}$ and $L_{X,\text{psr}}$ have a strong correlation with B_{lc} . In fact we found this correlation is as strong as the one with \dot{E} . It suggests that these two timing variables together may describe luminosities better. Unfortunately, large uncertainties in the fitting with currently available data hinder the progress towards this direction. Nonetheless, because synchrotron radiation luminosity depends on the magnetic field strength to the second power and on the energy distribution of emitting particles, the power indices of B_{lc} in Eq.(5) and Eq.(6), which are not close to 2, indicate that B_{lc} may play some role in determining energetics of those emitting particles, together with \dot{E} .

The flux ratio, $F_{X,\text{pwn}}/F_{X,\text{psr}}$, is not found to correlate with any timing properties. It indicates that, within the current uncertainty level, $L_{X,\text{pwn}}$ and $L_{X,\text{psr}}$ have a very similar dependence on pulsars' timing properties. This can also be seen from all the fitting results shown in Eqs.(1) – (6). It is, however, intriguing that $L_{X,\text{pwn}}$ seems to depend on \dot{E} or B_{lc} with a larger power index than $L_{X,\text{psr}}$ when considering \dot{E} and B_{lc} dependence separately. We note that this trend is not fully supported by the current statistics because of the large uncertainty, but it also appears in all the earlier literature as described in Section 1.

Another major discovery of this work is the dependence of Γ_{psr} on $\log T$, $\log P$ and $\log \dot{P}$. While the best fit of Γ_{psr} as a function of $\log P$ and $\log \dot{P}$ has $\chi^2_{\nu} = 25.12$, by adding one more variable, $\log T$, the best-fit χ^2_{ν} becomes 0.65. One can see that, from the F -test, it is a very significant improvement. From the fitting result, we suggest that Γ_{psr} is equal to a constant plus $\log(T^{-\frac{3}{2}}P^{-\frac{2}{3}}\dot{P}^{\frac{1}{3}})$ (Eq.(13)). If we consider this is synchrotron radiation emitted by a population of electron-positron pairs with a power-law energy distribution $N_E \propto E^{-\alpha}$, we have $\alpha = 2\Gamma_{\text{psr}} - 1$. Therefore α is equal to a constant plus $\log(T^{-3}P^{-\frac{4}{3}}\dot{P}^{\frac{2}{3}})$.

Non-thermal X-ray emissions from pulsars are proposed to emit by secondary pairs in the pulsar magnetosphere away from the stellar surface (e.g. Takata, Chang & Shibata (2008); Harding & Kalapotharakos (2015)). The production of these pairs can be just above the polar cap via one-photon pair production (Daugherty & Harding 1982) in the strong magnetic field close to pulsar's magnetic pole, or in the outer gap via two-photon pair production (Cheng, Ho & Ruderman 1986) in a thermal X-ray photon bath originating from the stellar surface. In the former scenario, curvature gamma-ray photons emitted by accelerated primary particles make

pairs through interactions with the ambient strong magnetic field. The energy of the created pairs is related to the energy of primary particles, which are accelerated by electric fields parallel to magnetic fields in the polar gap and at the same time may lose energy to surrounding thermal X-ray photons coming from the stellar surface through inverse Compton scattering (Chang 1995; Sturmer 1995; Harding & Muslimov 1998; Timokhin & Harding 2019). It is then possible that T plays a certain role in determining the energy distribution of the secondary pairs. In the latter scenario, since pairs are created in the outer gap through photon-photon collisions between curvature photons from primary particles and thermal X-ray photons from the stellar surface, it is obvious that surface temperature T plays a role in determining the energy distribution of the created secondary pairs, which, as well as for the case above the polar cap, of course also depends on energetics of primary particles. It in turn brings in the dependence on P and \dot{P} . Detailed modeling work is required to understand all these dependences.

The millisecond pulsar PSR J2124-3358 is an outlier in the P and \dot{P} distributions as shown in Fig. 1, but it fits pretty well into the 35 samples in the $L_{X,\text{pwn}}-\dot{E}$, $L_{X,\text{psr}}-\dot{E}$ and $L_{X,\text{pwn}}-L_{X,\text{psr}}$ relations and to a lower degree in the $L_{X,\text{pwn}}-B_{\text{lc}}$ and $L_{X,\text{psr}}-B_{\text{lc}}$ relations. It seems to indicate that millisecond pulsars share the same energy conversion physics with other ordinary pulsars, despite of their much shorter rotation periods and much larger characteristic ages. However, in the $\Gamma_{\text{psr}}-T$ distribution (Fig. 5), one can see that its non-thermal power-law spectrum is softer than the other 12 ordinary pulsars, even though its surface temperature is relatively high. Furthermore, if we include PSR J2124-3358 in the fitting of Γ_{psr} as a linear function of $\log T$, $\log P$ and $\log \dot{P}$, the best fit has $\chi^2_{\nu} = 8.44$, much larger than 0.65 obtained when only the 12 ordinary pulsars are included (Eq.(12)). This pulsar is not in the fundamental plane defined by Eq.(13).

We note that the spin-down power \dot{E} of PSR J2124-3358 is small. The maximum available potential drop to accelerate charged particles in pulsar's magnetosphere is proportional to $\dot{E}^{0.5}$ (see, e.g., Goldreich & Julian (1969); Ruderman & Sutherland (1975)). If the electric field to accelerate charged particles is not strong enough, the electrical acceleration may be balanced by the energy loss due to inverse Compton scattering against thermal photons (Chang 1995). One possibility is that there are two fundamental planes in the $\{\Gamma_{\text{psr}}, T, P, \dot{P}\}$ space. One is for those pulsars whose \dot{E} is large enough so that primary particles can reach high energies, and the other is for those with smaller \dot{E} whose primary particles can only reach a saturation energy, which is relatively lower. The energy distribution of radiating pairs is of course dependent on the energetics of primary particles. To verify this conjecture, more samples with smaller \dot{E} are desired.

ACKNOWLEDGEMENTS

This work is supported by the Ministry of Science and Technology (MOST) of the Republic of China (Taiwan) under grants MOST 108-2112-M-007-003 and MOST 109-2112-M-007-009.

DATA AVAILABILITY

The data underlying this article are available in the article and in the quoted references.

REFERENCES

- Abichandani, R., Mathur, M. B., Drake, J. J., Fruscione, A., Lee, N. P., Glotfelty, K. 2019, ATel 12463
- Abramowski et al. (H. E. S. S. Collaboration) 2012, A&A, 548, A46
- Archibald, R. F., Kaspi, V. M., Tendulkar, S. P., & Scholz, P. 2018, ApJ, 869, 180
- Becker, W., & Trümper, J. 1997, A&A, 326, 682
- Becker, W., Kramer, M., Jessner, A., et al. 2006, ApJ, 645, 1421
- Birzan, L., Pavlov, G. G., & Kargaltsev, O. 2016, ApJ, 817, 129
- Blumer, H., Safi-Harb, S., & McLaughlin, M. A. 2017, ApJL, 850, L18
- Bogdanov, S. 2013, ApJ, 762, 96
- Bogdanov, S. et al. 2019, ApJL, 887, L25
- Caswell, J. L., Kesteven, M. J., Stewart, R. T., Milne, D. K., & Haynes, R. F. 1992, ApJL, 399, L151
- Chang, C., Konopelko, A., & Cui, W. 2008, 682, 1177
- Chang, C., Pavlov, G. G., Kargaltsev, O., & Shibanov, Y. A. 2012, ApJ, 744, 81
- Chang, H.-K. 1995, A&A, 301, 456
- Cheng, K. S., Ho, C., Ruderman, M., 1986, ApJ, 300, 500
- Cheng, K. S., Taam, R. E., & Wang, W. 2004, ApJ, 617, 480
- Cheng, K. S., & Zhang, L. 1999, ApJ, 515, 337
- Chevalier, R. A. 2000, ApJ, 539, L45
- Dai, S., Johnston, S., Weltevrede, P., Kerr, M., Burgay, M., Esposito, P., Israel, G., Possenti, A., Rea, N., & Sarkissian, J. 2018, MNRAS, 480, 358
- Daugherty, J. K., & Harding, A. K. 1982, ApJ, 257, 603
- De Luca, A., Caraveo, P. A., Mereghetti, S., Negroni, M., & Bignami, G. F. 2005, ApJ, 623, 1051
- DeLaney, T., Gaensler, B. M., Arons, J., & Pivovarov, M. J. 2006, ApJ, 640, 929
- Duvidovich, L., Giacani, E., Castelletti, G., Petriella, A., & Supan, L. 2019, A&A, 623, A115
- Gaensler, B. M., Stappers, B. W., Frail, D. A., Johnston, S. 1998, ApJL, 499, L69
- Ge, M. Y., Lu, F. J., Yan, L. L., et al. 2019, Nature Astronomy, 3, 1122
- Giacani, E. B., Frail, D. A., Goss, W. M., & Vieytes, M. 2001, AJ, 121, 3133
- Goldreich, P., & Julian, W. H. 1969, ApJ, 157, 869
- Gotthelf, E. V. 2003, ApJ, 591, 361
- Gotthelf, E. V., & Halpern, J. P. 2008, ApJ, 681, 515
- Guillot, S., Kaspi, V. M., Archibald, R. F., et al. 2016, MNRAS, 463, 2612
- Harding, A. K., & Muslimov, A. G. 1998, ApJ, 508, 328
- Harding, A., Kalapotharakos, C., 2015, ApJ, 811, 63
- Helfand, D. J., Gotthelf, E. V., Halpern, J. P., et al. 2007, ApJ, 665, 1297H
- Hinton, J. A., Funk, S., Carrigan, S., Gallant, Y. A., de Jager, O. C., Kosack, K., Lemièrre, A., & Pühlhofer, G. 2007, A&A, 476, L25
- Huang, R. H. H., Kong, A. K. H., Takata, J., et al. 2012, ApJ, 760, 92
- Johnson, S. P., & Wang, Q. D. 2010, MNRAS, 408, 1216
- Kandel, D., Romani, R. W., An, H. 2019, ApJ, 879, 73
- Kargaltsev, O., Pavlov, G. G., & Garmire, G. P. 2007, ApJ, 660, 1413
- Kargaltsev, O., Pavlov, G. G., & Wong, J. A. 2009, ApJ, 690, 891
- Kaspi, V. M., Manchester, R. N., Johnston, S., Lyne, A. G., & D'Amico, N. 1992, ApJL, 399, L155
- Kennel, C. F., & Coroniti, F. V. 1984, ApJ, 283, 710
- Kishishita, T., Bamba, A., Uchiyama, Y., Tanaka, Y., & Takahashi, T. 2012, ApJ, 750, 162
- Klingler, N., Kargaltsev, O., Pavlov, G. G., et al. 2018, ApJ, 861, 5
- Klingler, N., Kargaltsev, O., Rangelov, B., et al. 2016a, ApJ, 828, 70
- Klingler, N., Rangelov, B., Kargaltsev, O., et al. 2016b, ApJ, 833, 253
- Kolb C., Blondin J., Slane P., Temim T., 2017, ApJ, 844, 1
- Kuiper, L., Hermsen, W., & Dekker, A. 2018, MNRAS, 475, 1238
- Li, X. H., Lu, F. J., & Li, T. P. 2005, ApJ, 628, 931
- Li, X.-H., Lu, F.-J., & Li, Z. 2008, ApJ, 682, 1166
- Lin, L. C.-C., Wang, H.-H., Li, K.-L., et al., 2018, ApJ, 866, 6
- Lyubarsky, Y. E. 2003, MNRAS, 345, 153
- Matheson, H., & Safi-Harb, S. 2010, ApJ, 724, 572
- Mattana, F., Falanga, M., Götz, D., et al. 2009, ApJ, 694, 12
- McGowan, K. E., Kennea, J. A., Zane, S., Cordova, F. A., Cropper, M., Ho, C., Sasseen, T., & Vestrand, W. T. 2003, ApJ, 591, 380
- Mignani, R.P., Razzano, M., Esposito, P., De Luca, A., Marelli, M., Oates, S. R., & Saz-Parkinson, P. 2012, A&A, 543, A130
- Ng, C. Y., Roberts, M. S. E., & Romani, R. W. 2005, ApJ, 627, 904
- Ng, C. Y., Romani, R. W., Briskin, W. F., Chatterjee, S., & Kramer, M. 2007, ApJ, 654, 487
- Pavan, L., Pühlhofer, G., Bordas, P., et al. 2016, A&A, 591, A91
- Pavlov, G. G., Zavlin, V. E., Sanwal, D., Burwitz, V., & Garmire, G. P. 2001, ApJ, 552, L129
- Petre, R., Kuntz, K. D., & Shelton, R. L. 2002, ApJ, 579, 404
- Posselt, B., Spence, G., & Pavlov, G. G. 2015, ApJ, 811, 96
- Posselt, B., Pavlov, G. G., Slane, P. O., et al. 2017, ApJ, 835, 66
- Possenti, A., Cerutti, R., Colpi, M., & Mereghetti, S. 2002, A&A, 387, 993
- Reynolds, S. P., Borkowski, K. J., & Gwynne, P. H. 2018, ApJ, 856, 133
- Roberts, M. S. E., Tam, C. R., Kaspi, V. M., et al. 2003, ApJ, 588, 992
- Romani, R. W., & Ng, C. Y. 2003, ApJ, 585, L41
- Romani, R. W., Ng, C. Y., Dodson, R., & Briskin, W. 2005, ApJ, 631, 480
- Romani, R. W., Slane, P., & Green, A. W. 2017, ApJ, 851, 61

- Ruderman, M. A., & Sutherland, P. G. 1975, *ApJ*, 196, 51
- Sakai, M., Matsumoto, H., Haba, Y., Kanou, Y., & Miyamoto, Y. 2013, *PASJ*, 65, 64
- Seward, F. D., & Wang, Z.-R. 1988, *ApJ*, 332, 199
- Sironi, L., Spitkovsky, A., Arons, J. 2013, *ApJ*, 771, 54
- Slane, P. 2017, Pulsar Wind Nebulae. In: Alsabti A., Murdin P. (eds) *Handbook of Supernovae*. Springer, Cham. https://doi.org/10.1007/978-3-319-21846-5_95
- Slane, P., Helfand, D. J., van der Swaluw, E., & Murray, S. S. 2004, *ApJ*, 616, 403
- Slane, P., Hughes, J. P., Temim, T. et al. 2012, *ApJ*, 749, 131
- Stappers, B. W., Gaensler, B. M., Johnston, S. 1999, *MNRAS*, 308, 609
- Sturmer, S. J. 1995, *ApJ*, 446, 292
- Takata J., Chang H.-K., Shibata S., 2008, *MNRAS*, 386, 748
- Takata, J., & Chang, H.-K. 2009, *MNRAS*, 392, 400
- Temim, T., Slane, P., Reynolds, S. P., Raymond, J. C., & Borkowski, K. J. 2010, *ApJ*, 710, 309
- Temim, T., Slane, P., Sukhbold, T., Koo, B.-C., Raymond, J. C., Gelfand, J. D. 2019, *ApJL*, 878, L19
- Timokhin, A. N., & Harding, A. K. 2019, *ApJ*, 871, 12
- Van Etten, A., Romani, R. W., & Ng, C.-Y., 2008, *ApJ*, 680, 1417
- Wilson, A. S. 1986, *ApJ*, 302, 718
- Zhang, L., & Cheng, K. S. 2003, *A&A*, 398, 639